Available online at www.sciencedirect.com
ScienceDirect
Ceramics International 37 (2011) 1801–1811
CERAMICS INTERNATIONAL
www.elsevier.com/locate/ceramint

Directional diffusion-controlled development of spinel interlayer between zinc-orthosilicate glaze and alumina

Chao-Hsien Wu [a], Chang-Ning Huang [a], Chao Sun [b], Cheng Kuan [b], Pouyan Shen [a,*]

[a] Department of Materials and Optoelectronic Science, National Sun Yat-sen University, Kaohsiung 80424, Taiwan
[b] Tien-Hsin Art and Pottery, No. 32-1 Tienshints, Sanchih, Taipei Hsien, Taiwan

Received 30 November 2010; received in revised form 12 January 2011; accepted 29 January 2011
Available online 9 March 2011

Abstract

Metal ion-doped zinc-orthosilicate crystalline glaze was overlain on α-Al_2O_3 polycrystals at 1270 °C followed by optional devitrification at 1080 °C for cross sectional electron microscopic characterization. An interlayer of gahnite spinel islands with varied Cr-dopant level, possibly in a formula of $Zn(CrAl)_2O_4$, was found to develop nonepitaxially at the glaze/substrate interface and follow parabolic growth kinetics due to outward diffusion of Al into the glaze. The spinel islands tended to coalesce with each other to form subgrain boundaries and were occasionally encompassed as nonepitaxial particles within the predominant willemite (α-Zn_2SiO_4) crystals in the glaze. A secondary Co- and Ti-containing gahnite spinel, possibly in a formula of $(ZnCoAl)(TiCoAl)_2O_4$, was found to nucleate epitaxially at the {1 1 1} junctions of the spinel islands when the glaze was further devitrified at 1080 °C. There is negligible glaze infiltration into the substrate or thermal-mismatch induced cracking across the interphase interface, implying potential thermal bonding/sealing applications of the present glaze for alumina-based ceramics.

Keywords: A. Firing; B. Defects; Zinc orthosilicate glaze; Alumina substrate; Spinel interlayer

1. Introduction

The addition of ZnO and some nucleation agents, such as titanic acid [1], to the silicate melt has been commonly used to fabricate partially crystallized ware glaze tailored with brilliant lath-like crystals of willemite (α-Zn_2SiO_4) [2]. The crystalline ware glaze has a rather complicated crystallization behavior due to the thickness constraint and the viscous flow of the glaze on the pottery bodies which are typically polycrystalline ceramic materials made from clay minerals enriched with an Al_2O_3 component. Recently, electron microscopy and nondestructive confocal imaging techniques with submicron spatial resolution capability have been used to reveal fine details of the amorphous phase separation region at the center of the spherulites and at the interface of impinged spherulites in terms of lath-like willemite crystallites [3]. (Under the constraint of the glaze thickness, the willemite crystallites were found to develop into flattened spherulites, which consist of lath-like crystals growing in the order of $[0\ 0\ 0\ 1] \gg \langle 1\ 0\ \bar{1}\ 0\rangle > \langle 2\ \bar{1}\ \bar{1}\ 0\rangle$ and viable for coalescence over the $\langle 2\ \bar{1}\ \bar{1}\ 0\rangle$ habit plane [3].) Thermal cycle etching of willemite (0 0 0 1) due to the underlying effects of surface premelting, dislocation outcrops and polygonization was also studied [4]. However, the extent of interdiffusion that affects the formation of the bonding interlayer at the glaze/substrate interface and thermal-mismatch induced cleaving-healing, if any, among the co-existing phases were not reported.

Solid-state diffusional coating on polycrystals commonly causes a diffusion zone with specified phase assemblages and crystallographic relationships [5–9]. Defect clusters may also occur for ionic crystals if aliovalent or size-mismatch ions are involved in the diffusion couples [10]. The composite thus formed at high temperatures may be vulnerable upon cooling to have further phase and/or microstructural changes. For examples, thermal mismatch of co-existing phases [11]

* Corresponding author. Tel.: +886 7 5254060; fax: +886 7 5254099.
E-mail address: pshen@mail.nsysu.edu.tw (P. Shen).

0272-8842/$36.00
doi:10.1016/j.ceramint.2011.03.004

and polymorphic phase change of a dispersed phase [12] were found to cause extensive cleaving and spontaneous healing of the matrix phase. The cleaving–healing process also accounts for (*h k l*)-specific precipitation in some natural minerals, such as rutile in garnet of crustal metamorphic rock [13] and ultra-high pressure terrane [14]. The reequilibration of solids in the presence of a fluid phase was further elucidated to involve the generation of porosity in the product phase and interface-coupled dissolution–reprecipitation [15]. It is of interest to find out whether a bonding interlayer of specific phase and defect microstructures can be formed when a molten zinc-orthosilicate glaze is overlain on a ceramic substrate.

Here we report the formation of a special kind of spinel interlayer when a metal ions-doped zinc-orthosilicate glaze was overlain on α-Al_2O_3 polycrystals. We focused on: (1) directional diffusion-controlled nucleation and growth of the islands of Cr-containing gahnite spinel in the interlayer; (2) nonepitaxial incorporation of the spinel islands into willemite that was predominantly crystallized in the glaze; (3) the occurrence of a secondary spinel that was dissolved with various metal ions and nucleated epitaxially at specific surface junctions of the spinel islands when the glaze was further devitrified at a specified supercooling condition; and (4) rather limited glaze infiltration into the substrate and negligible thermal-mismatch induced cracking/cleaving for potential thermal bonding applications.

2. Experimental

The powdery glaze with 28.3ZnO, 51.2SiO_2, 4.1TiO_2, 5.4Na_2O, 4.1CaO, 2.5K_2O, 2.1TiO_2, 1.2CoO and 1.1Al_2O_3 in mol% was doped with 0.1 and 1 wt.% Cr_2O_3 (Cerac, 325 mesh, 99.99% pure) in order to study the effect of Cr content

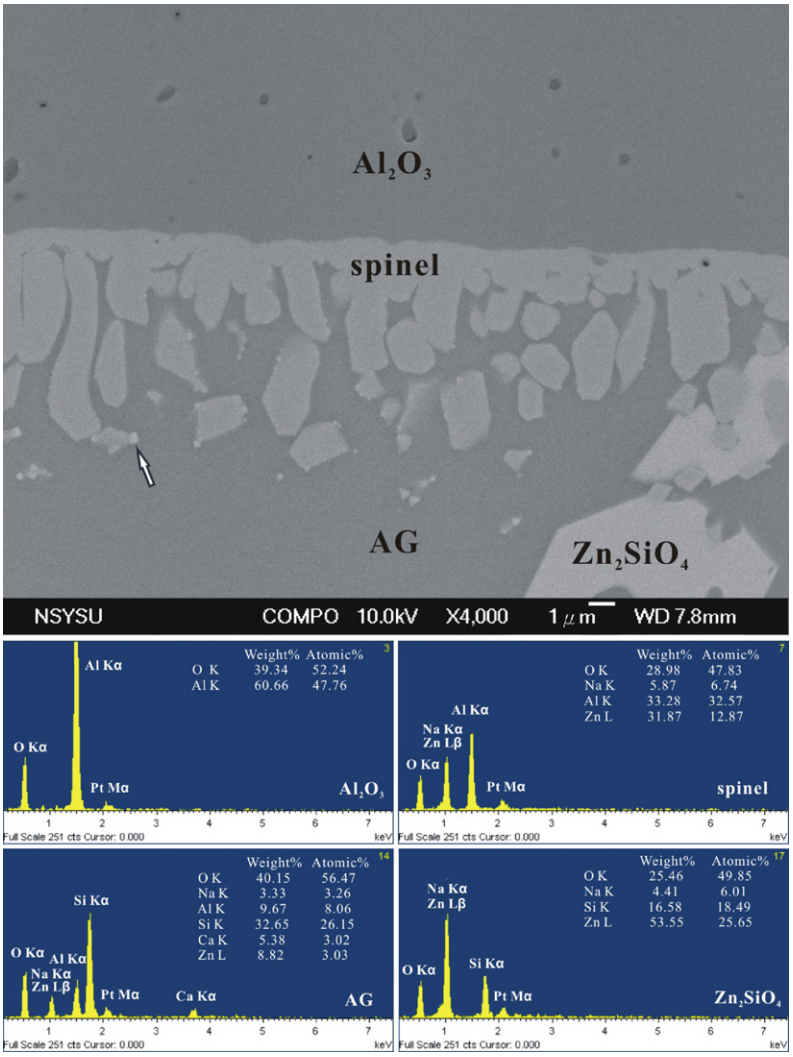

Fig. 1. SEM (BEI) showing the cross section of zinc orthosilicate glaze (with 0.1% Cr) overlain on polycrystalline α-alumina at 1270 °C for 1 h followed by devitrification at 1080 °C for 5 h. The corresponding point-count EDX spectra were taken from Al_2O_3, Cr-containing gahnite spinel islands, amorphous glaze (AG) and α-Zn_2SiO_4 more or less with counts contribution from each other. Note some micron-sized spinel islands were encompassed in the coarsened α-Zn_2SiO_4 crystal and submicron-sized secondary spinel particles with bright contrast (indicated by an arrow) were nucleated from the faceted primary spinel islands (cf. text). The Pt counts are due to platinum coating.

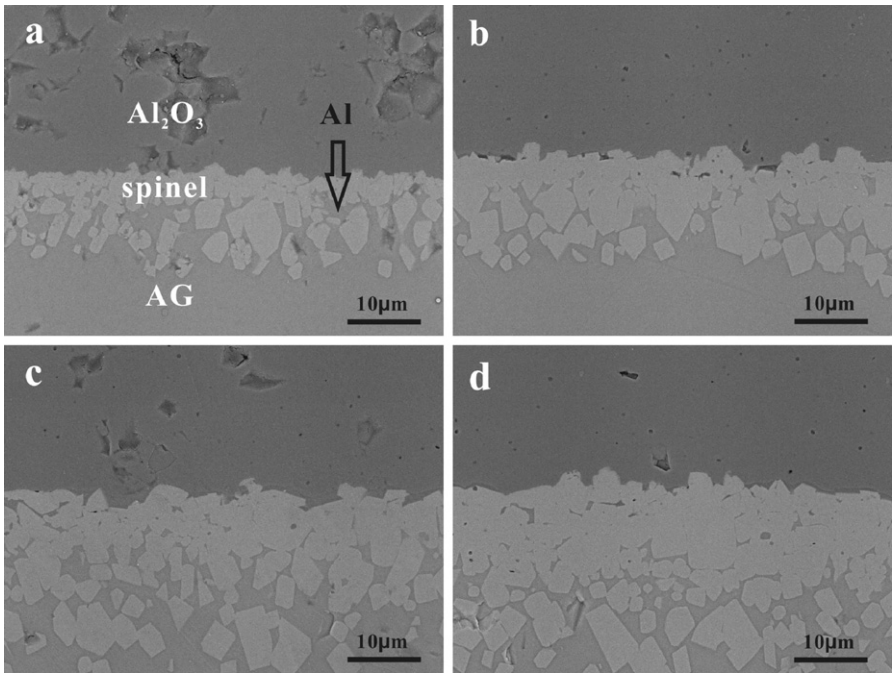

Fig. 2. SEM (BEI) cross section view of zinc orthosilicate glaze (with 0.1% Cr) overlain on polycrystalline α-alumina at 1270 °C for (a) 5 h, (b) 10 h, (c) 15 h and (d) 20 h showing progressive widening of the spinel interlayer by outward flux of Al (arrow) from α-alumina into amorphous glaze (AG) following a parabolic rate law (cf. text).

on the formation of the chromium spinel interlayer when the glaze was overlain on an alumina substrate at high temperatures. The powders thus combined were thoroughly mixed in de-ionized water in a beaker by magnetic stirrer and then oven-dried at 110 °C for 2–3 h. The resultant slurry was sprayed on a flat substrate of corundum (α-Al_2O_3) polycrystals (prepared by solid-state sintering of Al_2O_3 powders (Cerac, 99.99% pure) at 1600 °C for 12 h) and then fired in an open air furnace at 1270 °C for 1 h followed by cooling to room temperature in the furnace. Alternatively, the slurry doped with 0.1 wt.% Cr and sprayed on the same substrate was fired at 1270 °C for 5 up to 20 h and then quenched in air to study progressive widening of the spinel interlayer upon glazing. For a comparison of the spinel phase, the glaze fabricated at 1270 °C for 1 h was further devitrified at 1080 °C for 5 h and then cooled in the furnace.

The glaze samples overlain on α-Al_2O_3 polycrystals were cross sectioned and then polished followed by platinum coating for scanning electron microscopic (SEM, JEOL JSM-6700F at 10 kV) study under back-scattered electron image (BEI) mode coupled with energy dispersive X-ray (EDX) analysis. Focused ion beam (FIB, SII NanoTechnology Inc. SMI 3050, using Ga ion beam) was used to make 10 μm thick sections across the glaze/substrate interface for analytical electron microscopy (AEM, JEOL 3010 at 200 kV or 300 kV) studies. Transmission electron microscopy (TEM) based on selected area electron diffraction (SAED) coupled with bright field image (BFI), dark field image (DFI) and EDX was used to identify defect microstructures and compositions of the individual crystalline phases. Lattice imaging coupled with 2-D Fourier transform was used to characterize lattice imperfections and fringe spacings of the epitaxial spinel phases.

3. Results

3.1. Cross sectional SEM observations

Cross sectional BEI indicated the glaze samples overlain on α-Al_2O_3 polycrystals are ca. 80–100 μm in thickness regardless of the Cr dopant level and firing conditions. Point count EDX analyses on the glaze samples doped with 0.1 (Fig. 1) and 1 wt.% Cr (Appendix 1) further revealed the α-Al_2O_3 substrate, the α-Zn_2SiO_4 crystals in the glaze and an interlayer of spinel islands at the glaze/substrate interface. Some of the spinel islands turned out to be Cr-containing gahnite according to later AEM analysis. The spinel islands were more or less impinged with each other or with the predominant α-Zn_2SiO_4 crystals in the glaze. Submicron-sized secondary spinel with bright contrast in BEI due to dissolution of various transition metal cations, as indicated by later AEM analysis, was found to attach to the spinel islands. Such secondary spinel particles were observed in the samples subjected to devitrification at 1080 °C (Fig. 1 and Appendix 1), but not in the sample quenched from 1270 °C (Fig. 2). Prolonged dwelling for 5 up to 20 h at 1270 °C (Fig. 2) caused progressive widening of the spinel interlayer due to outward diffusion of Al as discussed later.

3.2. AEM

The crystal structures, lattice relationship and defect microstructures of the co-existing phases in the partially devitrified glaze were further revealed by AEM. Fig. 3a shows the TEM BFI of the α-Al_2O_3 polycrystals in the substrate and the spinel interlayer nearby. The BFI (Fig. 3b) and corresponding SAED pattern (Fig. 3c) taken from individual α-Al_2O_3 grain in the $[1\ \bar{1}\ 0\ \bar{1}]$ zone axis indicated the substrate does not have definite crystallographic relationship with the spinel islands. High-angle grain boundaries and triple junctions characteristic to solid-state sintering remained unchanged for the α-Al_2O_3 substrate regardless of the firing conditions. EDX analysis (not shown) indicated the α-Al_2O_3 grains do not uptake appreciable alloying elements from the glaze.

The spinel island formed at 1270 °C was identified by BFI (Fig. 3d) and SAED pattern (Fig. 3e) to be of spinel structure having well-developed {1 1 1} faces exposed to the amorphous glaze as viewed edge on in the [1 1 0] zone axis. The {1 1 1} faces of the spinel were also identified to be inclined when viewed in the [1 1 1] zone axis (Appendix 2). These primary spinel islands tended to coalesce with each other to show misfit dislocations at the subgrain boundaries with rather complicated diffraction contrast as indicated by BFI (Fig. 4a) and weak-beam DFI (Fig. 4b).

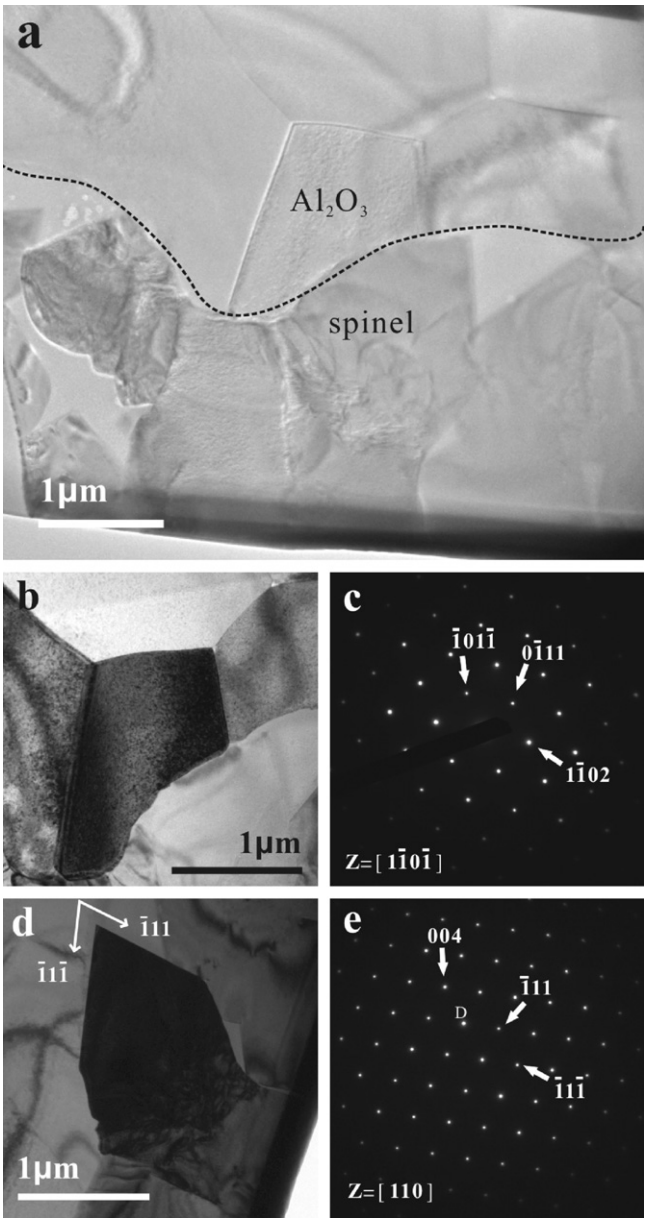

Fig. 3. TEM (a) cross section BFI of the spinel interlayer in zinc orthosilicate glaze (with 1% Cr) overlain on polycrystalline α-Al_2O_3 at 1270 °C for 1 h followed by devitrification at 1080 °C for 5 h, (b,c) and (d,e) BFI and corresponding SAED pattern taken from the α-Al_2O_3 and the spinel tilted to the $[1\ \bar{1}\ 0\ \bar{1}]$ and [1 1 0] zone axes, respectively. The double diffraction is denoted as D in (e).

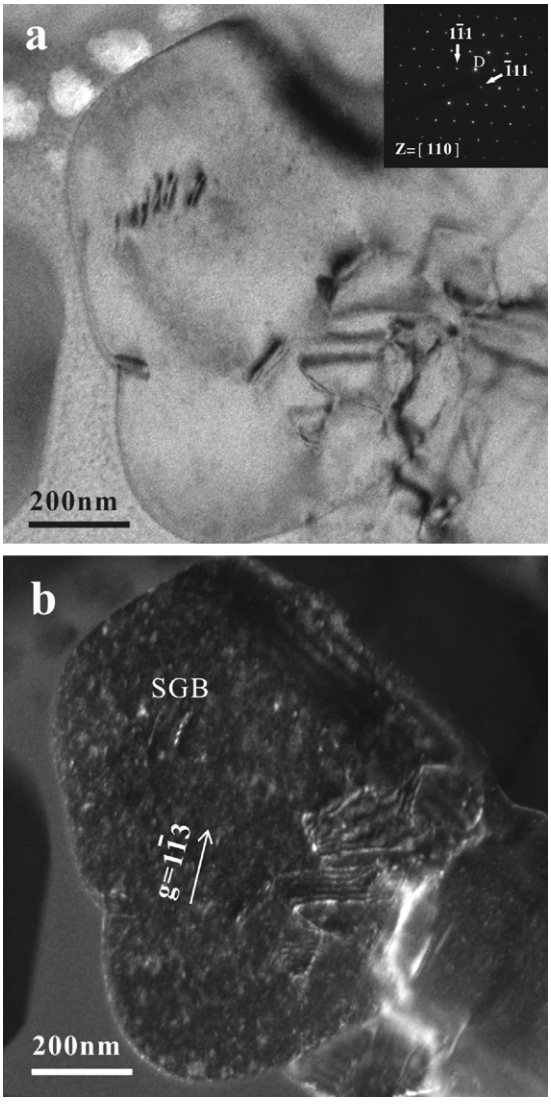

Fig. 4. TEM (a) BFI and corresponding SAED pattern (inset with double diffraction denoted as D) of the primary spinel particles having been coalesced to have nearly the same orientation in the [1 1 0] zone axis, (b) weak-beam DFI ($g = 1\ \bar{1}\ 3$) of the spinel with dislocations at its subgrain boundaries (SGB). The same specimen as in Fig. 3.

Secondary spinel particles formed by devitrification at 1080 °C as mentioned were identified to follow parallel epitaxial relationship with the primary spinel islands as shown by the TEM BFI (Fig. 5a) and SAED pattern (Fig. 5b) of a representative case. DFI using the superimposed $(1\ \bar{1}\ 3)$ diffractions of the two spinels (Fig. 5c) showed misfit dislocations at the interphase interface. Lattice imaging coupled with 2-D Fourier transform of the primary spinel island (Fig. 5d) and secondary spinel (Fig. 5e), showed further details of the dislocation-free interior with a $(1\ \bar{1}\ 1)$

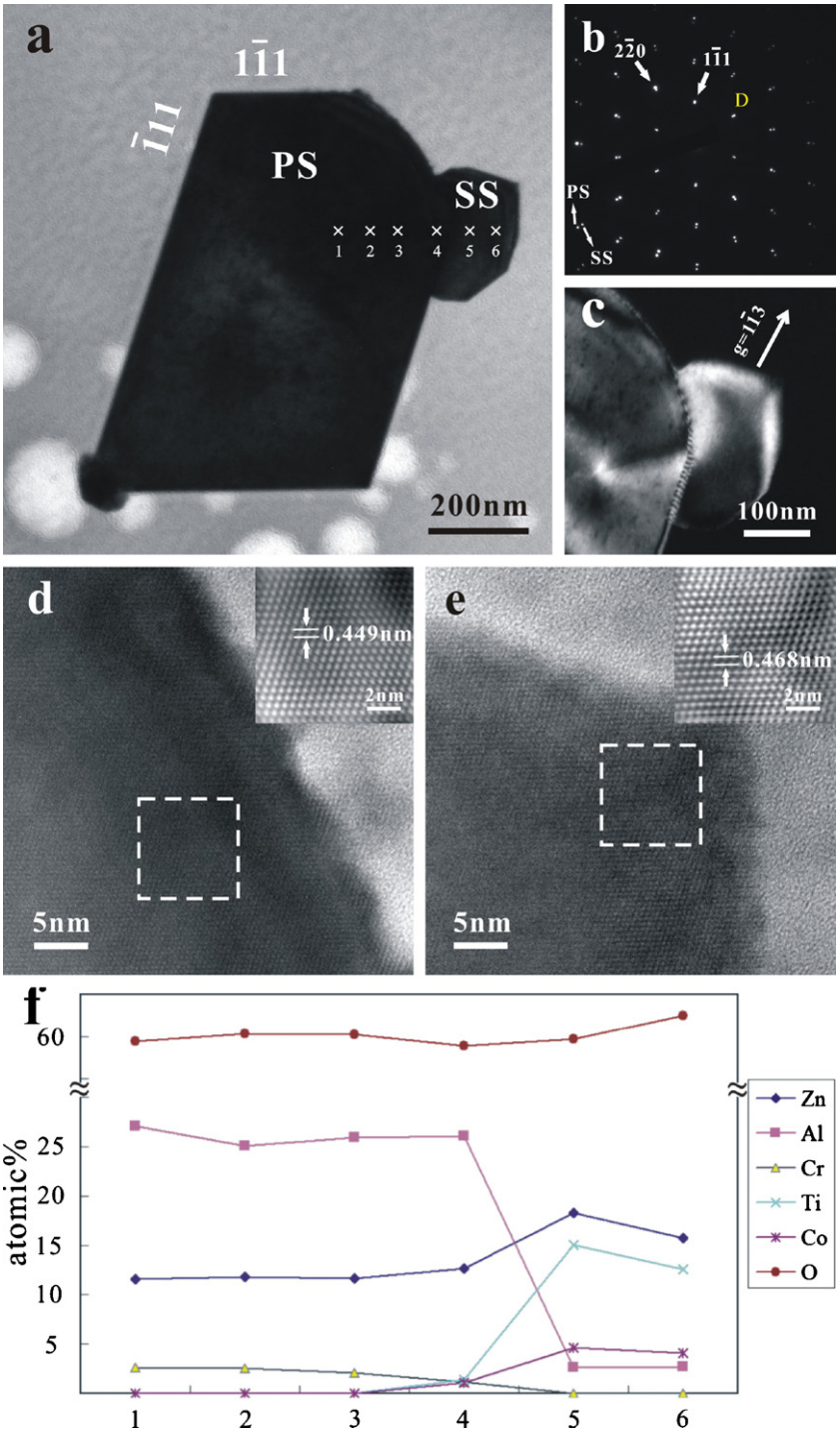

Fig. 5. TEM (a) BFI and (b) SAED pattern of submicron-sized Co- and Ti-containing gahnite secondary spinel (designated as SS) parallel epitaxially nucleated from relatively large sized and Cr-containing gahnite primary spinel (designated as PS), (c) DFI ($g = 1\ \bar{1}\ 3$ of PS and SS) showing misfit dislocations at the interphase interface and defect clusters in PS not SS, (d) and (e) lattice images coupled with Fourier transform images (insets) from the square regions of PS and SS, showing dislocation free interior with $(1\ \bar{1}\ 1)$ d-spacings of 0.449 and 0.468 ± 0.002 nm, respectively, (f) composition profiles across the PS/SS interface due to interdiffusion (cf. text). The same specimen as in Fig. 3.

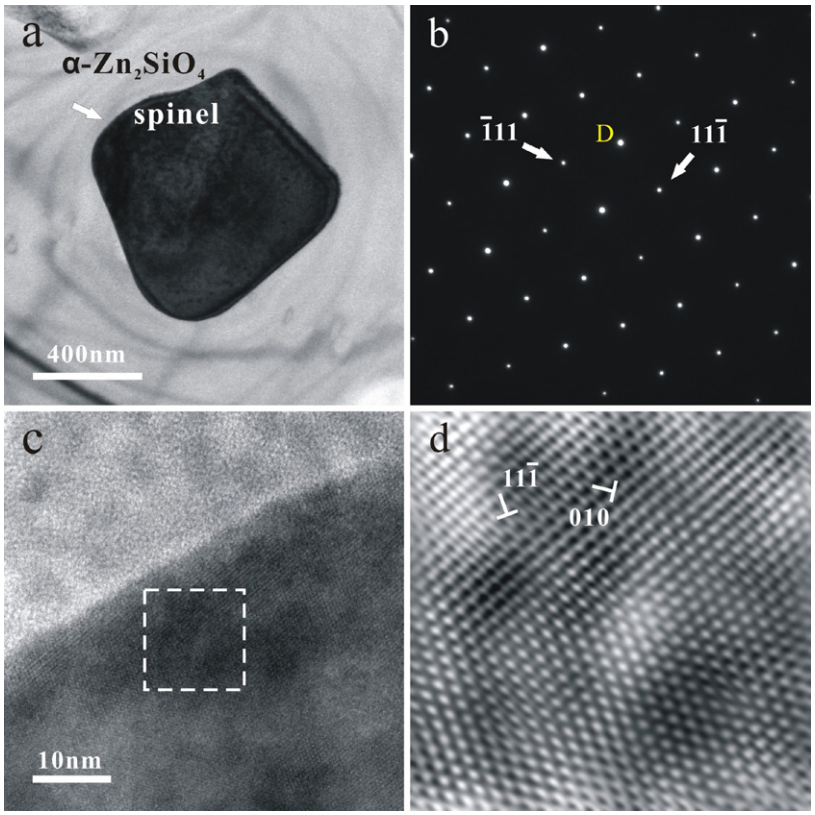

Fig. 6. TEM (a) BFI and (b) SAED pattern of a primary spinel particle in the [1 0 1] zone axis which was encompassed nonepitaxially within a coarsened α-Zn_2SiO_4 crystal with strain contrast. (c) Lattice image of the spinel edge arrowed in (a) coupled with (d) 2-D Fourier transform of the square region showing dislocations with half planes parallel to (0 1 0) and (1 1 $\bar{1}$). The same specimen as in Fig. 3.

d-spacing of 0.449 and 0.468 ± 0.002 nm, respectively. The composition profiles based on point-count EDX analyses (see Appendix 3 for the representative EDX spectra) across the interface of the two spinel phases (Fig. 5f) showed that the spinel island is in fact Cr-containing gahnite possibly in a formula of $Zn(CrAl)_2O_4$ whereas the secondary spinel with a bright contrast in BEI (cf. Fig. 1 and Appendix 1) is Co- and Ti-containing gahnite possibly in a formula of $(ZnCoAl)(TiCoAl)_2O_4$ as discussed later in Section 4.1. There is significant decrease of Al and Cr content accompanied with the increase of Zn, Ti and Co content from the spinel island toward the secondary spinel due to interdiffusion across the interface.

The spinel islands also tended to be encompassed nonepitaxially within the coarsened α-Zn_2SiO_4 crystal. Fig. 6a and b shows such a case where the incorporated spinel was tilted to an exact zone axis for strong Bragg diffraction in BFI, yet the α-Zn_2SiO_4 host in poor orientation with considerable strain contrast due to slight thermal mismatch as discussed later. The spinel island remained {1 1 1} faceted despite the constraint of the α-Zn_2SiO_4 host. Lattice imaging (Fig. 6c) coupled with 2-D Fourier transform (Fig. 6d) near the edge of thus constrained spinel showed abundant dislocations having half plane parallel to its (1 1 $\bar{1}$) and (0 1 0) lattice planes.

4. Discussion

4.1. Structure formula of primary and secondary spinel

It is difficult if not impossible to do single-crystal X-ray structural Rietveld refinement on the primary and secondary spinel islands which are as small as submicron size with varied dopant level and distributed only at the glaze/substrate interface. Electron paramagnetic resonance (EPR) spectroscopic study of cation distribution and inversion parameter of the spinel is also beyond the scope of this work. Nevertheless point-count EDX analysis and electron diffraction of the spinel phases in various zone axes gave unambiguous chemical composition and lattice parameter, as compiled in Table 1, for the following discussion on the possible chemical formula and exact lattice mismatch of the spinel phases.

The stoichiometric $ZnAl_2O_4$ has normal spinel type structure with Zn^{2+} and Al^{3+} in coordination number (CN) of 4 and 6, respectively [16]. Such an ideal gahnite has negligible degree of cation disorder according to thermodynamic measurements [17,18] and experimental results [19]. The present AEM results indicated some of the primary spinel islands are Cr-containing gahnite, which is possibly in a formula of $Zn(CrAl)_2O_4$ in view of recent crystal chemistry

Table 1
Observed and refined d spacings for the primary and secondary spinels in Fig. 5a.

Primary spinel			Secondary spinel	
$h\,k\,l$	Obsd	Refined	Obsd	Refined
1 1 1	0.470	0.470	0.488	0.489
2 2 0	0.287	0.288	0.298	0.299
3 1 1	0.247	0.246	0.257	0.255
2 2 2	0.235	0.235	0.245	0.244
4 0 0	0.205	0.204	0.213	0.212
3 3 1	0.187	0.187	0.194	0.194
4 2 2	0.167	0.166	0.174	0.173
5 1 1	0.158	0.157	0.164	0.163
4 4 0	0.144	0.144	0.150	0.150

The observed d spacings (nm) based on SAED patterns in various zone axis of the epitaxial spinel particles in Fig. 5a are accurate within ±0.002 nm. The refined d spacings of the primary spinel (a = 0.815 nm) and secondary spinel (a = 0.847 nm) are also given.

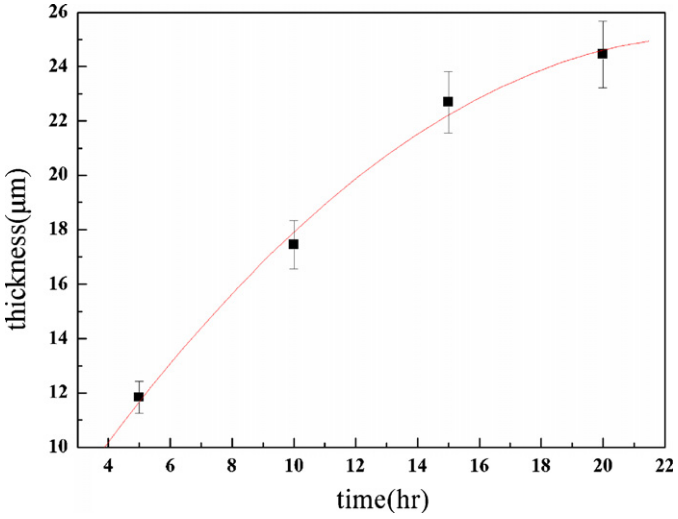

Fig. 7. Thickness as a function of firing time at 1270 °C for the spinel interlayer between the metal ion-added orthosilicate glaze and alumina substrate indicating parabolic growth kinetics (cf. text).

study of Cr-spinel minerals [20]. The substitution of Cr^{3+} (0.0615 nm) for Al^{3+} (0.0535 nm) in CN 6 having their effective ionic radii [21] in parenthesis would cause distortion of the residence sites. It is noteworthy that additional X-ray diffraction from a number of primary spinel islands (Appendix 4) gave a lattice parameter (a = 0.8085 ± 0.0001 nm) nearly the same as that reported for pure gahnite (a = 0.8086 nm, JCPDS file 74-1136). This indicates that Cr content is rather limited or even negligible for most of the primary spinel islands.

As for the secondary spinel, it is Co- and Ti-containing gahnite possibly in a formula of $(ZnCoAl)(TiCoAl)_2O_4$. In this connection, EPR spectroscopy results indicated that a general formula of Co^{2+}-doped gahnite can be written as $^{IV}[Zn_{1-x}Co_{x-\delta}Al_{\delta}]^{VI}[Al_{2-\delta}Co_{\delta}]O_4$, where x represents the level of incorporated Co^{2+} in the gahnite structure, and δ is the inversion parameter of the spinel structure [22]. (The inversion parameter in fact increases with Co^{2+} doping level [22].) The additional Ti^{4+} dopant may prefer the octahedral site in the oxygen framework of gahnite-based spinel analogous to the case of rutile-type titania [13,14]. The co-substitution of Ti^{4+} (0.0605 nm) and Co^{2+} (0.065 nm) for Al^{3+} (0.0535 nm) in CN 6 with effective ionic radii [21] in parenthesis may be favored by a fair size mismatch and a charge compensating effect. Detailed EPR study of cation distribution is required to clarify whether such a substitution scheme indeed occurs for the secondary spinel. In any case, the cation-vacancy induced defect clusters are negligible in the present spinel phases as paracrystalline distribution of defect clusters would otherwise form like the case of nonstoichiometric $Co_{3-\delta}O_4$ [23] and Zr^{4+}-doped $Co_{3-\delta}O_4$ [10].

There are regularly spaced misfit dislocations at the interface of the primary spinel (designated as PS) and the secondary spinel (denoted as SS) due to a rather large lattice mismatch $\varepsilon = (a_{SS} - a_{PS})/a_{PS}$. Such a constrained lattice mismatch was calculated to be 4% according to the refined lattice parameters (a_{SS} = 0.815 nm and a_{PS} = 0.847 nm, cf. Table 1) based on SAED patterns of the epitaxial spinel particles.

4.2. Formation mechanism of primary and secondary spinel

The primary spinel interlayer was formed by a directional diffusion-controlled nucleation and growth process when the glaze was molten on the alumina polycrystals. Such primary spinel islands could be nonepitaxially nucleated at the alumina grain boundaries for beneficial lower activation energy [24]. Alternatively, the ZnO_4 and AlO_6 units in the molten glaze as in the case of calcium zinc aluminosilicate glasses [25], may cause bulk nucleation of Cr-containing gahnite $Zn(CrAl)_2O_4$ crystals having Zn^{2+} and Cr^{3+} in tetrahedral and octahedral sites, respectively. Since the original Al content in the glaze is less than 2 wt.%, the primary spinel would not nucleate except near the Al^{3+} main source, i.e., the alumina substrate. The primary spinel islands thus nucleated should have random orientation as confirmed by XRD (Appendix 4).

Upon prolonged dwelling at the firing temperature of 1270 °C, the primary spinel islands were significantly coarsened and accumulated as an interlayer (Fig. 2) following parabolic growth rate law (Fig. 7), i.e., $L(t) \propto t^{1/2}$ where L is the thickness of the layer at a specified firing time (t) [26]. Such parabolic growth kinetics is justified by directional diffusion, i.e., outward diffusion of Al^{3+} from the substrate and inward supply of Zn^{2+} and Cr^{3+} from the molten glaze to form the spinel interlayer. The spinel growth rate was thus affected by the viscosity of the molten glaze at 1270 °C, i.e., a considerably supercooled condition comparing with the cotectic melting points (1315 and 1425 °C) in the simpler ternary composition of SiO_2–ZnO–Al_2O_3 [27]. It should be noted that molten silica tended to infiltrate the alumina polycrystals along the grain

boundaries [28]. The primary spinel interlayer however has effectively restricted glaze infiltration as a silica liquid film would otherwise form along the grain boundaries of α-Al_2O_3 polycrystals. (The AEM-EDX spectra taken from the substrate grain boundaries always showed Al and O counts but no appreciable Si counts.) Apparently the spinel islands more or less coalesced in a close packed manner have effectively hindered the inward diffusion of Si as well as other components, i.e., Zn, Ti, Co, Ca, Na, K, Cr from the molten glaze. The outward diffusion of Al from the solid substrate into the molten glaze appeared to be rapid enough to cause instantaneous nucleation and growth of the interlayer spinel in the glaze to control further diffusion. This may be due to a higher grain-boundary diffusivity of Al^{3+} than Si^{4+} in the α-Al_2O_3 substrate and/or the spinel interlayer.

The secondary $(ZnCoAl)(TiCoAl)_2O_4$ spinel particles having parallel epitaxial relationship with the Cr-containing $ZnAl_2O_4$ spinel islands in the interlayer occurred only for the glaze samples devitrified at 1080 °C regardless of the Cr dopant level in the glaze. This indicates that the secondary spinel particles were newly nucleated from the primary spinel islands upon devitrification of the glaze. The {1 1 1} junction rather than the well-developed {1 1 1} surface or less developed {1 0 0} surface of the Cr-containing $ZnAl_2O_4$ crystal appeared to be the favorable nucleation site of the secondary spinel. In this connection, it is of interest to note that a diamond nucleation site responsible for epitaxial growth of diamond on silicon by chemical vapor deposition was identified in high-resolution TEM images [29]. The diamond crystallites were found to grow partially epitaxially on Si {1 1 1}, whereas perfect heteroepitaxially (parallel) at {1 1 1} junction or 1° off at {1 1 1}/{1 0 0} junction of the Si substrate [29].

4.3. Incorporation of spinel islands in coarsened willemite

Eutectic or cotectic growth, as allowed under specified temperature and composition conditions of the SiO_2–ZnO–Al_2O_3 ternary [27], is expected to cause epitaxial composite [24] and hence cannot explain the gahnite-based spinel islands being encompassed nonepitaxially in willemite (Fig. 6). Instead, the nonepitaxial incorporation of spinel islands in willemite can be reasonably explained by a much larger growth rate of willemite than the refractory spinel oxide when they impinged in the molten glaze at 1270 °C. The relatively small spinel particles would exert a considerable dragging effect on the willemite growth front until detachment occurred.

Upon detachment, the willemite host failed to modify the {1 1 1} faces of the incorporated spinel islands to follow its habit plane, i.e., $(2\ \bar{1}\ \bar{1}\ 0)$ [3]. This implies that the spinel {1 1 1} face has a lower surface energy than the habit plane of willemite. Thermally activated rotation of the intragranular particles may enable their reorientation toward a specific crystallographic relationship with respect to the matrix for an interfacial energy favorable state as experimentally proved in a number of ceramic composite systems such as zirconia crystal grains with embedded $Ni_{1-x}O$ or $Co_{1-x}O$ particles [30,31]. It is an open question whether prolonged firing above a critical temperature would urge the encompassed spinel islands to reach epitaxial relationship with the willemite host.

4.4. Negligible cracking along the interphase interface

Furnace cooling or even air quenching did not cause appreciable cracking/cleaving at the glaze/substrate interface or various crystal interfaces. Apparently, thermal and phase transformation induced cleaving, as prevailed in a number of ceramic composite [11,12] and natural metamorphic rocks [13,14], did not happen in the present crystalline glaze composite. In this regard, the thermal expansion coefficient differs little for the present phases, i.e., $\sim 7.5 \times 10^{-6}\ K^{-1}$ for α-Al_2O_3 [32], $\sim 5.5 \times 10^{-6}\ K^{-1}$ for α-Zn_2SiO_4 [33], $8.7–9.9 \times 10^{-6}\ K^{-1}$ for $ZnAl_2O_4$ [34] (presumably valid also for the present primary and secondary spinels containing various amount of dopants) and $4.2–9.2 \times 10^{-6}\ K^{-1}$ for soda lime or alkaline earth alumino-silicate glass [35]. Thus, the thermal expansion coefficient difference among the phases is not large enough to cause appreciable cracking/cleaving along the interface of the adjoined phases when the crystalline glaze on α-Al_2O_3 polycrystals was rapidly cooled to room temperature in air.

5. Conclusions

In essence, an interlayer consisting of Cr-containing gahnite spinel islands was developed nonepitaxially at the glaze/alumina interface when metal ions-added zinc orthosilicate glaze was overlain on alumina at 1270 °C. The spinel interlayer follows a parabolic growth rate due to directional Al diffusion from the solid substrate to the molten glaze. A secondary Co- and Ti-containing gahnite spinel was further nucleated parallel epitaxially from the {1 1 1} junctions of the spinel islands when the glaze was devitrified at 1080 °C to form more α-Zn_2SiO_4 crystals. The spinel islands remained {1 1 1} facetted despite the nonepitaxial confinement by the host α-Zn_2SiO_4 crystal. A rather limited process of melt infiltration into the substrate or negligible thermal-mismatch induced cracking across the interphase interface may allow potential thermal bonding/sealing applications of the present glaze for alumina-based ceramics such as sapphire or ruby.

Acknowledgements

Meanwhile this paper was written and submitted, Cheng Kuan passed away. Chao Sun and Pouyan Shen would like to dedicate this article to her memory. We thank an anonymous referee for constructive comments. Supported by the Center for Nanoscience and Nanotechnology of NSYSU and National Science Council, Taiwan ROC.

Appendix 1

SEM (BEI) showing the cross section of zinc orthosilicate glaze (with 1% Cr) overlain on polycrystalline α-Al_2O_3 at 1270 °C for 1 h followed by devitrification at 1080 °C for 5 h. The corresponding point-count EDX spectra were taken from Al_2O_3, Cr-containing gahnite spinel islands, amorphous glaze (AG) and α-Zn_2SiO_4 more or less with counts contribution from each other. Note some micron-sized spinel islands were encompassed in the coarsened α-Zn_2SiO_4 crystal and submicron-sized secondary spinel particles with bright contrast (indicated by an arrow) were nucleated from the faceted islands of primary spinel (cf. text). The Pt counts are due to platinum coating.

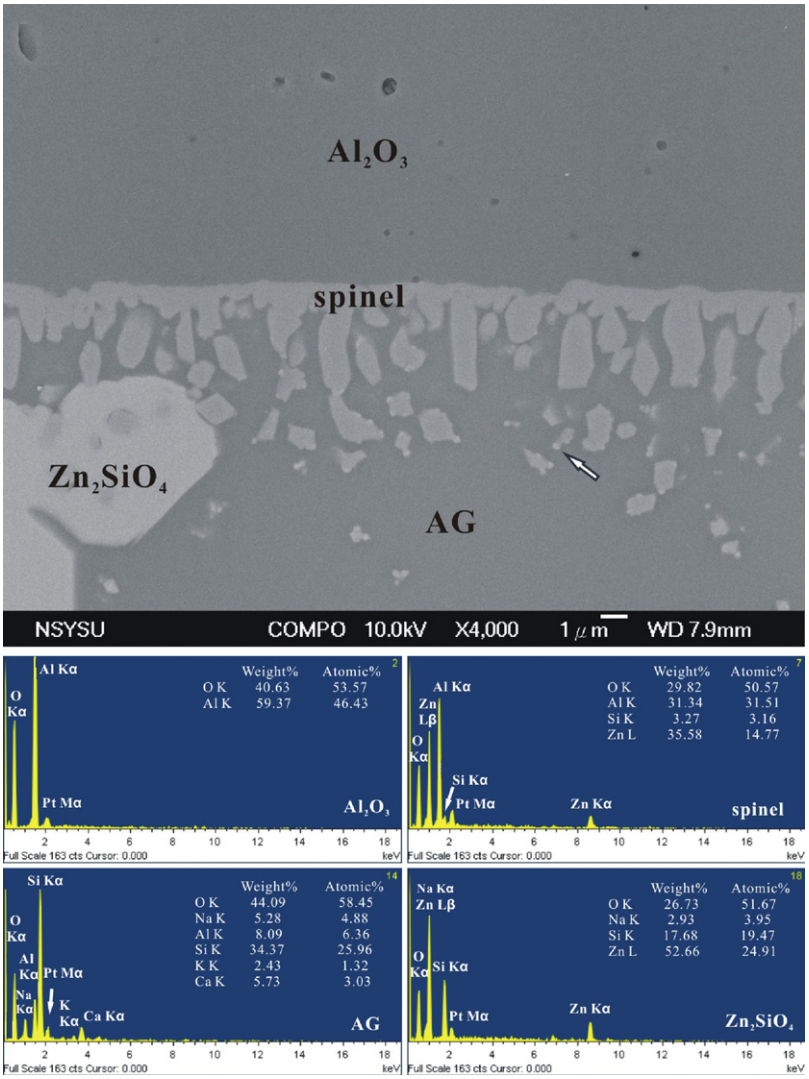

Appendix 2

TEM (a) BFI with SAED pattern (inset) and (b) DFI ($g = \bar{2}\ 0\ 2$) of the Cr-containing $ZnAl_2O_4$ spinel island in the [1 1 1] zone axis having the inclined {1 1 1} surfaces exposed to amorphous glaze (AG). The same specimen as in Fig. 3.

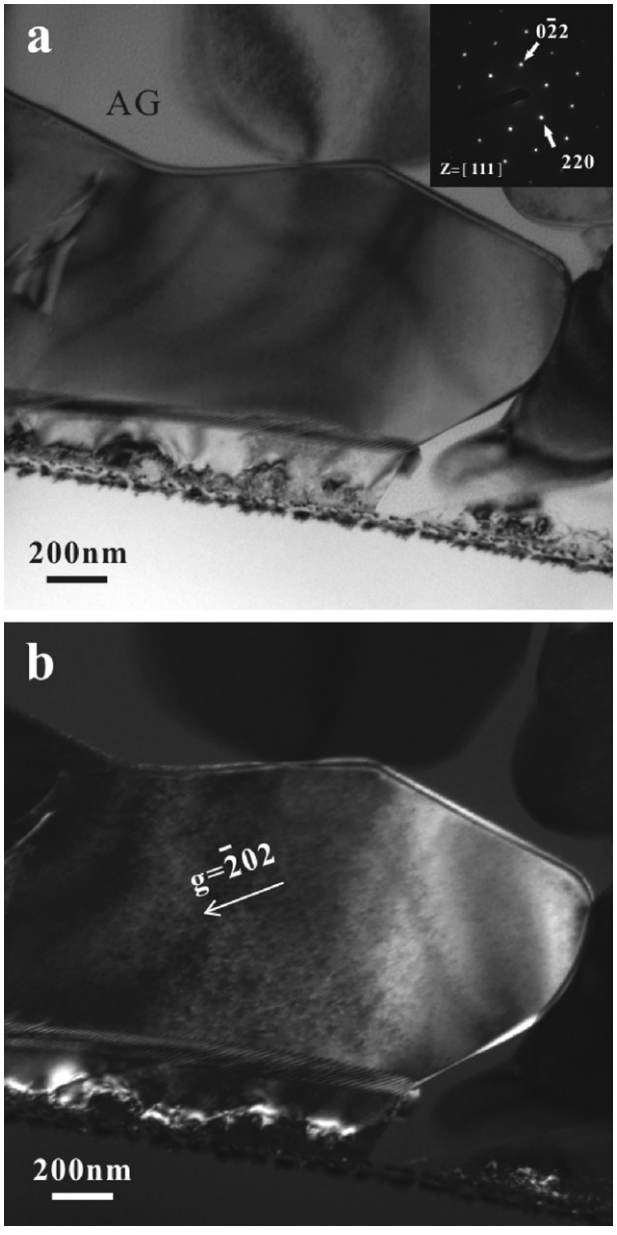

Appendix 3

EDX spectrum of (a) Cr-containing gahnite spinel, (b) Co- and Ti-containing secondary spinel, i.e., analysis points 1 and 6, respectively in Fig. 5f.

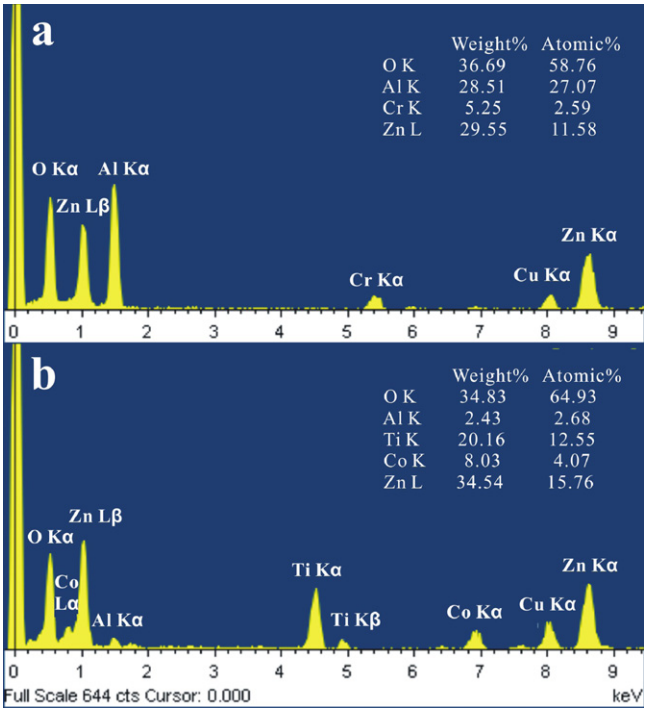

Appendix 4

X-ray diffraction trace CuKα using Siemens D5000 diffractometer at a scanning rate of 0.36°/min (step size 0.03°, fixed counts 5 s) of the alumina (denoted as a) substrate and spinel (denoted as sp) interlayer beneath the zinc orthosilicate glaze doped with 1% Cr. This sample was fired at 1270 °C for 20 h followed by devitrification at 1080 °C for 5 h and then polishing to expose the predominant primary spinel islands. Note the secondary spinel was hardly detected and the primary spinel has a refined lattice parameter of $a = 0.8085 \pm 0.0001$ nm (cf. Table 2) despite Cr content variation from 0 to 2.5 at.% among the spinel islands (cf. text).

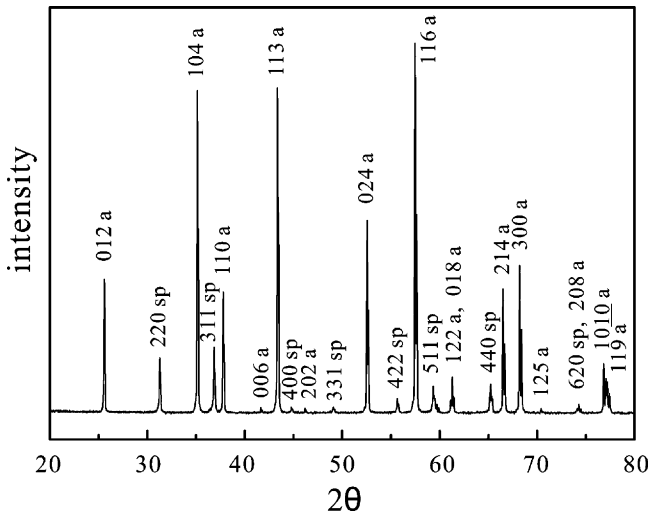

Table 2
Observed and calculated *d* spacings (nm) for the primary spinel islands based on XRD trace in Appendix 4.

h k l	Obsd	Refined
2 2 0	0.2857	0.2859
3 1 1	0.2437	0.2438
4 0 0	0.2022	0.2021
3 3 1	0.1856	0.1855
4 2 2	0.1651	0.1650
5 1 1	0.1556	0.1556
4 4 0	0.1430	0.1429
6 2 0	0.1279	0.1278

References

[1] W.H. Zimmer, Crystallized glazes, Trans. Am. Ceram. Soc. 4 (1902) 38.
[2] F.H. Norton, The control of crystalline glazes, J. Am. Ceram. Soc. 20 (1937) 217.
[3] C. Sun, C. Kuan, F.J. Kao, Y.M. Wang, J.C. Chen, C.C. Chang, P. Shen, On the nucleation, growth and impingement of plate-like α-Zn_2SiO_4 spherulites in glaze layer: a confocal and electron microscopic study, Mater. Sci. Eng. A 379 (2004) 327–333.
[4] P.T. Chao, P. Shen, C.C. Lin, Thermal cycle etching of willemite (0 0 0 1): effects of surface premelting, dislocation outcrops and polygonization, Mater. Sci. Eng. A 335 (2002) 191–197.
[5] P. Shen, D. Gan, C.C. Lin, Microstructures and crystallographic relationships in aluminized coatings on Rene 80, Mater. Sci. Eng. 78 (1986) 171–178.
[6] P. Shen, D. Gan, C.C. Lin, Superlattice of beta phase in aluminized coatings on Rene 80, Mater. Sci. Eng. 78 (1986) 163–170.
[7] P. Shen, D. Gan, C.C. Lin, Microstructures of first-stage aluminized coating on Rene 80, Mater. Sci. Eng. 82 (1986) 197–202.
[8] S.L. Hwang, P. Shen, Microstructures and crystallographic relationships in aluminized coatings on IN713LC and MAR-M247, Mater. Sci. Eng. 94 (1987) 243–250.
[9] P. Shen, C.C. Chou, M.J. Tsai, C.C. Lin, Superlattice of the beta phase in aluminized coatings on IN713LC and MAR-M247, Mater. Sci. Eng. 87 (1987) 145–149.
[10] M.Y. Li, P. Shen, On the nucleation and paracrystal interspacing of Zr-doped $Co_{3-\delta}O_4$, Mater. Sci. Eng. B 111 (2004) 82–89.
[11] W.H. Lee, P. Shen, Thermal-mismatch induced cleaving and spontaneous healing of zirconia dispersed $Co_{1-x}O$, Mater. Sci. Eng. A 332 (2002) 262–269.
[12] M.Y. Li, P. Shen, S.L. Hwang, Transformation-enabled cleaving and healing in zirconia dispersed $Co_{1-x}O$, Mater. Sci. Eng. A 386 (2004) 104–111.
[13] S.L. Hwang, P. Shen, T.F. Yui, H.T. Chu, TiO_2 nanoparticle trails in garnet: implications of inclusion pressure-induced microcracks and spontaneous metamorphic-reaction healing during exhumation, J. Metamorph. Geol. 25 (2007) 451–460.
[14] S.L. Hwang, T.F. Yui, H.T. Chu, P. Shen, H.P. Schertl, R.Y. Zhang, J.G. Liou, On the origin of oriented rutile needles in garnet from UHP eclogites, J. Metamorph. Geol. 25 (2007) 349–362.
[15] A. Putnis, C.V. Putnis, The mechanism of reequilibration of solids in the presence of a fluid phase, J. Solid State Chem. 180 (2007) 1783–1786.
[16] J.C. Waerenborgh, H. Annersten, T. Ericsson, M.O. Figueiredo, J.M.P. Cabral, A Mossbauer study of natural gahnite spinels showing strongly temperature-dependent quadrupole splitting distributions, Eur. J. Mineral. 2 (1990) 267–271.
[17] A. Navrotsky, O.J. Kleppa, The thermodynamics of cation distributions in simple spinels, J. Inorg. Nucl. Chem. 29 (1967) 2701–2714.
[18] H.St.C. O'Neill, A. Navrotsky, Simple spinels: crystallographic parameters, cation radii, lattice energies, and cation distribution, Am. Mineral. 68 (1983) 181–194.
[19] N. Kashii, H. Maekawa, Y. Hinatsu, Dynamics of the cation mixing of $MgAl_2O_4$ and $ZnAl_2O_4$ spinel, J. Am. Ceram. Soc. 82 (1999) 1844–1848.
[20] D. Lenaz, A. De Min, G. Garuti, F. Zaccarini, F. Princivalle, Crystal chemistry of Cr-spinels from the lherzolite mantle peridotite of Ronda (Spain), Am. Mineral. 95 (2010) 1323–1328.
[21] R.D. Shannon, Revised effective ionic radii and systematic studies of interatomic distances in halides and chalcogenides, Acta Crystallogr. A 32 (1976) 751–767.
[22] J. Popović, E. Tkalčec, B. Gržeta, S. Kurajica, B. Rakvin, Inverse spinel structure of Co-doped gahnite, Am. Mineral. 94 (2009) 771–776.
[23] W.H. Lee, P. Shen, $Co_{3-\delta}O_4$ paracrystal: 3-D assembly of nano-size defect clusters in spinel lattice, J. Solid State Chem. 177 (2004) 101–108.
[24] D.A. Porter, K.E. Easterling, M.Y. Sherif, Phase Transformations in Metals and Alloys, 3rd ed., CRC Press, Boca Raton, 2009.
[25] A.A. Omar, S.A.M. Abdel-Hameed, Crystallization of calcium zinc aluminosilicate glasses, Ceram. Sisikáty 53 (2009) 171–179.
[26] C. Wagner, Contributions to the theory of surface colouring of metals, Z. Phys. Chem. B 21 (1933) 25–41.
[27] R. Hansson, B. Zhao, P.C. Hayes, E. Jak, A reinvestigation of phase equilibria in the system Al_2O_3–SiO_2–ZnO, Metall. Mater. Trans. B 36 (2005) 187–193.
[28] Y. Kuromitsu, H. Yoshida, H. Takede, K. Morinaga, Interaction between alumina and binary glasses, J. Am. Ceram. Soc. 80 (1997) 1583–1587.
[29] S.T. Lee, H.Y. Peng, X.T. Zhou, N. Wang, C.S. Lee, I. Bello, Y. Lifshitz, A nucleation site and mechanism leading to epitaxial growth of diamond films, Science 287 (2000) 104–106.
[30] J. Chen, P. Shen, On the rotation of nonepitaxy $Ni_{1-x}O$ particles within zirconia grain, Scripta Mater. 37 (1997) 1287–1294.
[31] K.T. Lin, P. Shen., Thermally activated rotation of $Co_{1-x}O$ particle within zirconia grains, Mater. Sci. Eng. A 270 (1999) 125–132.
[32] C.J. Engberg, E.H. Zehms, Thermal expansion of Al_2O_3, BeO, MgO, B_4C, SiC, and TiC above 1000 °C, J. Am. Ceram. Soc. 42 (1958) 300–305.
[33] G.K. White, R.B. Roberts, Thermal expansion of willemite, Zn_2SiO_4, Aust. J. Phys. 41 (1988) 791–795.
[34] A. Petric, H. Lingw, Electrical conductivity and thermal expansion of spinels at elevated temperatures, J. Am. Ceram. Soc. 90 (2007) 1515–1520.
[35] R.H. Doremus, Glass Science, John Wiley and Sons, New York, 1973, p. 102.